Proceedings of the ASME 2010 3rd Joint US-European Fluids Engineering Summer Meeting and 8th International Conference on Nanochannels, Microchannels, and Minichannels
FEDSM-ICNMM2010
August 1-5, 2010, Montreal, Canada

FEDSM-ICNMM2010-30419

PREDICTION OF RESIDUAL STRESS IMPROVEMENT BY WATER JET PEENING USING CAVITATING JET SIMULATION WITH BUBBLE FLOW MODEL

Masashi Fukaya
Hitachi, Ltd.
832-2, Horiguchi, Hitachinaka,
Ibaraki, Japan

Ren Morinaka
Hitachi-GE Nuclear Energy, Ltd.
5-2-2, Omika-cho, Hitachi-shi,
Ibaraki, Japan

Noboru Saitou
Hitachi, Ltd.
3-1-1, Saiwai-cho, Hitachi-shi,
Ibaraki, Japan

Hisamitsu Hatou
Hitachi, Ltd.
3-1-1, Saiwai-cho, Hitachi-shi,
Ibaraki, Japan

Yoshiaki Tamura
Toyo University
2100, Kujirai, Kawagoe,
Saitama, Japan

Yoichiro Matsumoto
University of Tokyo
7-3-1, Hongo, Bunkyo-ku, Tokyo,
Japan

ABSTRACT

We developed the new method for predicting a region of compressive residual stress on the weld surface after water jet peeing (WJP), which is a preventive maintenance technology for nuclear power plants. A cavitating jet is impinged on the weld surfaces of structures in a nuclear reactor. Bubble collapse impact causes plastic deformation of the weld surface, and changes the residual stress from tensile to compressive. Compressive residual stress prevents the occurrence of stress corrosion cracking (SCC) on the weld surface. A cavitating jet vertically injected into a submerged flat plate was investigated. Tensile stress was introduced onto the surface of the stainless steel plate by grinding before WJP in the experiment. We numerically simulated impulsive bubble pressure that varied by microseconds in the cavitating jet with the "bubble flow model". The bubble flow model simulates the abrupt time-variations in the radius and inner pressure of bubbles based on the Rayleigh-Plesset equation in a cavitating flow. The cavitation collapse energy was estimated based on the bubble pressure. The cavitation collapse energy was compared with the measured compressive residual stress on the flat plate after WJP. The radial range of the compressive residual stress from the jet center axis is one of the most important measures of performance of WJP. The radial range of the cavitation collapse energy corresponded to that of compressive residual stress with a prediction error of +/- 20% under different conditions of jet velocity and the distance between the jet nozzle and plate surface. The results confirmed that the method we developed for predicting the region of compressive residual stress after WJP was valid.

INTRODUCTION

Water Jet Peening (WJP) is a practical technology for preventive maintenance based on the effective use of cavitation. Hitachi, Ltd. has applied WJP to 16 nuclear power plants in Japan since 1999. The welds of structures in nuclear reactors are subjected to tensile residual stress without any surface treatment. Stress corrosion cracking (SCC) may occur on the weld surfaces if the material conditions of tensile residual stress, sensitization, and a corrosive environment are simultaneously satisfied. WJP changes the tensile residual stress of the welds to compressive residual stress and prevents SCC (1-5).

A nozzle attached to the tip of a robot's arm is inserted into a reactor vessel filled with water in WJP. A high-speed water jet is injected from the nozzle by a high-pressure pump. Cavitation occurs in the low-pressure regions in the flow; therefore, the cavitating jet is generated. The cavitating jet is impinged on the weld surface of structures. The cavitation bubbles collapse generating shock waves and a micro-jet near the weld (6). The shock waves and the micro-jet hit the weld surface and the impact causes plastic deformation changing the residual stress from tensile to compressive. The nozzle is controlled to shift the position of the cavitating jet so that it covers the area where residual stress improvement is required.

The improvement of the residual stress by cavitation has been reported in experiments (1-5, 7, and 8). The flow and the bubble behaviors of cavitating jets have been experimentally studied (9, 10). The shock waves in fluid and the elastic stress waves in a solid have been numerically simulated, which were caused by a bubble collapse near the wall (11). However, no numerical flow simulations have yet been applied to cavitating jets to estimate the residual stress. We developed a new numerical method of predicting the region of compressive residual stress on weld surfaces after WJP.

We numerically simulated bubble behaviors in a cavitating jet with the "bubble flow model", where many tiny spherical bubbles are initially assumed to exist in the flow. The bubble radius varies with the pressure difference between the bubbles and their surrounding water. The abrupt time-variations in the bubble radius and the bubble pressure are calculated with the Rayleigh-Plesset equation (12). The bubble nuclei distribution is also calculated in the bubble flow model. We simulated impulsive bubble pressure that varied by microseconds in the cavitating jet, and then estimated the cavitation collapse energy based on the bubble pressure and the bubble nuclei distribution.

We predicted the cavitation erosion area around the impeller of a centrifugal pump using the same simulation code as that in the previous studies (13, 14). We confirmed a high correlation between the estimated cavitation collapse energy and the plastic deformation on the impeller blade surface, which was formed by cavitation bubble collapse. The change in the residual stress was caused by plastic deformation on the weld surface in WJP. Therefore, the high correlation between the estimated cavitation collapse energy and the compressive residual stress is also promising.

We verified the prediction accuracy of residual stress by comparing the cavitation collapse energy with the measured residual stress after WJP in the present study. From the viewpoint of reducing the time for WJP in nuclear reactors, broader areas of the residual stress improvement is desirable at each cavitating jet position. We focused on the radial range of compressive residual stress from the jet center axis when the cavitating jet was vertically injected to a submerged flat plate. The radial range of cavitation collapse energy was compared with that of compressive residual stress to verify the accuracy of prediction.

NOMENCLATURE

E: Cavitation collapse energy (J), (J/m^3)
f: Volume fraction (-)
n: Bubble number density (m^{-3})
p: Pressure (Pa)
r: Bubble radius (m)
R: Radial range from jet center axis (m)
t: Time (s)
Δt: Time step (s)
T: Surface tension (N/m)
ΔT: Total calculation time (s)
u: Velocity (m/s)
U: Contravariant velocity (m/s)
ΔV: Volume of numerical mesh (m^3)
κ: Specific heat ratio (-)
μ: Viscosity (Pa s)
ρ: Density of water (kg/m^3)

Subscripts

cal: Calculation
exp: Experiment
surf: Surface
B: Bubble
G: Gas phase
L: Liquid phase
th: Threshold
v: Vapor

NUMERICAL METHOD

Governing Equations

We made three main assumptions concerning the bubbles in a non-compressible liquid in the bubble flow model.

(a) The gas phase consisting of spherical bubbles is compressible.
(b) No collision or coalescence occurs. The bubbles are filled with vapor and non-condensable gas. Mass transfer between the gas and the water is negligibly small compared to the liquid mass.
(c) The density and momentum of the gas phase are sufficiently small to be negligible.

The governing equations are described as follows in the general coordinate system (15). The momentum conservation equation for the bubble flow is

$$\frac{\partial(\rho_L f_L u_{Li})}{\partial t} + J\frac{\partial(\rho_L f_L u_{Li} U_{Li}/J)}{\partial \xi_j} = -\nabla_i p + \nabla_j(\mu \nabla_j u_{Li}) + \frac{1}{3}(\mu \nabla_k u_{Lk}) \quad . \quad (1)$$

The conservation of bubble number density is

$$\frac{\partial n_G}{\partial t} + J\frac{\partial(n_G U_{Gi}/J)}{\partial \xi_j} = 0 \quad . \quad (2)$$

The pressure equation is

$$\frac{1}{c^2}\frac{\partial p}{\partial t} + \nabla_j f_L u_{Lj} + \nabla_j f_G u_{Gj} - 4\pi r_G{}^2 n_G \frac{Dr_G}{Dt} = 0 \quad . \quad (3)$$

Equation (3) is obtained based on pseudo-compressibility, which is derived from the conservation of volumetric fractions and the conservation of bubble number density.

The volumetric motion of an isolated bubble is described by the Rayleigh-Plesset equation,

$$r_G \frac{D^2 r_G}{Dt^2} + \frac{3}{2}\left(\frac{Dr_G}{Dt}\right)^2 = \frac{p_B - p_L}{\rho_L} \quad , \quad (4)$$

$$p_B = p_G + p_v - \frac{2T}{r_G} - 4\mu\frac{1}{r_G}\frac{Dr_G}{Dt} \quad , \quad (5)$$

$$p_G r_G^{\,3} = const. \quad \left(\frac{Dr_G}{Dt} > 0\right) \text{ , and} \quad (6)$$

$$p_G r_G^{\,3\kappa} = const. \quad \left(\frac{Dr_G}{Dt} < 0\right) \text{ ,} \quad (7)$$

where both T (= 0.072 N/m) and p_v (= 2300 Pa) are constant. The non-condensable gas pressure, p_G, varies with isothermal expansion and adiabatic contraction (Eqs. (6) and (7)). The specific heat ratio, κ, is 1.4. The effects of evaporation and condensation on the surface of a bubble are modeled according to the pressure variations in the non-condensable gas (16). The viscosity, μ, in Eq. (5) is assumed to be the same as that of water ($\mu = 1.0 \times 10^{-3}$ Pa s).

The void fraction is calculated from the bubble radius and the bubble number density by

$$f_G = \frac{4}{3}\pi r_G^{\,3} n_G \quad . \quad (8)$$

Equation (8) means that the void fraction increases when the bubble expands or where bubble nucluei have accumulated.

The velocity difference between the liquid and the bubble, i.e., the slip velocity, was not taken into account in the present simulation. There were no turbulent models used in the simulation code to reduce the calculation time.

Cavitation Collapse Energy

The energy released at bubble collapse is defined as

$$E = k\sum p_{ci}^{\,2} \quad , \quad (9)$$

where p_c is the bubble collapse pressure and k is a proportionality constant (17). While the bubbles did not vanish or generate the shock waves in the present simulation, the predicted bubble pressure was qualitatively related to the bubble collapse pressure (13, 14). We therefore numerically investigated the cavitation collapse energy by defining

$$E = \sum p_{Bi}^{\,2} (n_G \Delta V) \ , \quad (10)$$

where k is assumed to be 1.0. The bubble pressure represents the bubble collapse pressure in Eq. (10). The $n_G \Delta V$ means the number of bubbles in each numerical mesh.

Boundary and Initial Conditions

Figure 1 shows a numerical mesh. The simulated region was limited between the nozzle and the flat plate, where the submerged cavitating jet from the nozzle impinged vertically on the plate. We assumed an axisymmetric flow field and conducted calculations within a range of 2 degrees in the θ direction using periodic boundary conditions since the nozzle and the flat plate shapes were axisymmetric. The nozzle had a cylindrical throat and a horn-shaped flow passage downstream of the throat. The nozzle throat diameter was 2 mm. The length and the expansion angle of the horn-shaped flow passage were 11 mm and 30 degrees. The cartesian mesh was prepared in the

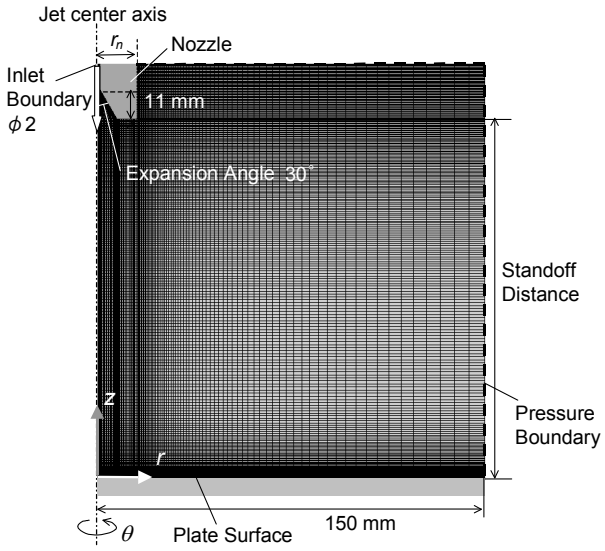

Fig. 1 Simulated region and boundary conditions

Table 1 Boundary and initial conditions

Case	Inlet Velocity (m/s)	Standoff Distance (mm)	Boundary Pressure (Pa)	Initial Bubble Radius (m)
1	254.6	140	3.0×10^5	7.0×10^{-6}
2	254.6	140	1.0×10^5	1.0×10^{-5}
3	254.6	100	1.0×10^5	1.0×10^{-5}
4	197.3	100	1.0×10^5	1.0×10^{-5}
5	98.7	100	1.0×10^5	1.0×10^{-5}

r-z plane except for the horn-shaped flow passage.

The pressure boundary conditions are plotted on the dotted line in Fig. 1, and a constant pressure of 3.0×10^5 Pa or 1.0×10^5 Pa was assumed. There are uniform velocity conditions at the nozzle inlet. The inlet velocity and the distance between the nozzle edge and the flat plate, i.e., the standoff distance, were changed as listed in Table 1. There are non-slip velocity conditions on the solid surfaces of the nozzle and the flat plate.

The initial void fraction was 0.001. The initial conditions of the bubble radius were 7.0×10^{-6} m or 1.0×10^{-5} m, which were assumed by taking into consideration the pressure upstream of the nozzle in the experiment. The boundary and initial conditions are summarized in Table 1.

RESULTS AND DISCUSSION

Flow Pattern and Bubble Behavior

The flow pattern and the bubble behavior in Case 1 are explained in this section by using Figs. 2-5. The flow pattern and the bubble behavior were unsteady. Figures 2-5 show the instantaneous results. When WJP is conducted in a nuclear reactor, the water depth of the weld and the nozzle is over 20 m

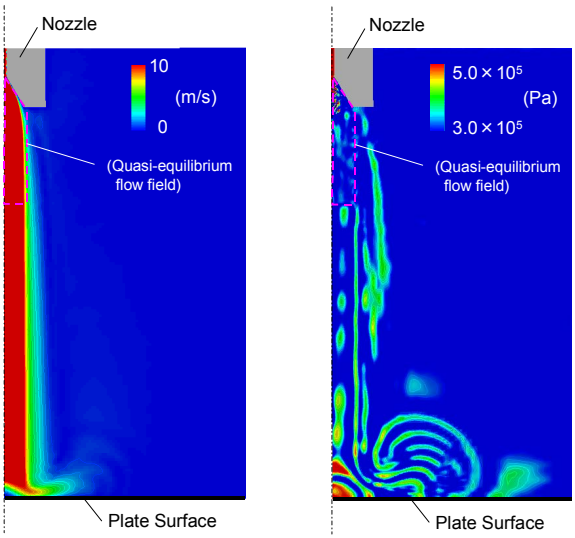

(a) Velocity (b) Pressure

Fig. 2 Velocity and static pressure of water in Case 1

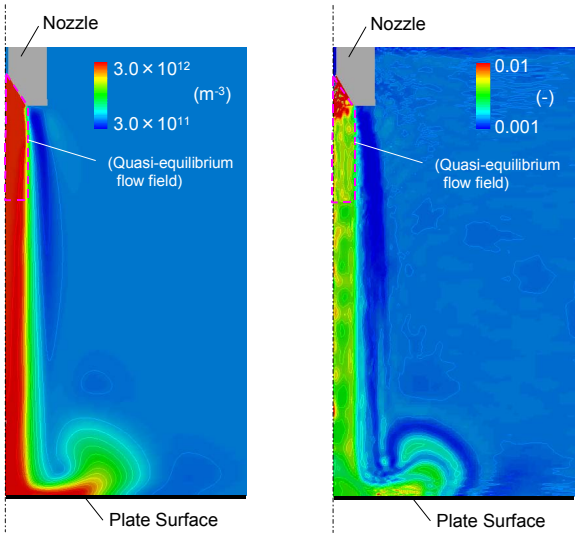

(a) Bubble number density (b) Void fraction

Fig. 3 Bubble number density and void fraction in Case 1

in some cases. Then, the boundary pressure in Case 1 was 3.0×10^5 Pa. The calculation of bubble pressure diverged around the nozzle. We assumed quasi-equilibrium between the bubble pressure and its surrounding pressure of water in the numerically unstable flow field instead of solving Eqs. (4)-(7).

Figure 2 shows the velocity and the static pressure of water in Case 1. The water jet injected from the nozzle impinged on the flat plate, and the water flowed along the plate while rolling up. The unsteadiness was not strong since the flow vortex structure was not sufficiently simulated. The static pressure varied with a strong unsteadiness affected by the bubble behavior through the fourth term of Eq. (3).

Figure 3 shows the bubble number density and the void fraction. The bubble nuclei were distributed in the jet and near the flat plate within a radial range from the jet center axis. The void fraction depends on the distribution of the bubble number density and the bubble radius, as shown in Eq. (8). The void fraction increased in the jet, which means that a cavitating jet was generated.

Figure 4 shows the bubble pressure abruptly fluctuated in and around the main flow. Figure 4 (b) shows the transient bubble pressure near the flat plate at point A in Fig. 4 (a). The bubble pressure impulsively increased in about 5 microseconds during the motion of the bubble shrink. Even though the bubbles shrank abruptly, they rebounded without collapsing in the simulation. Sato et al. observed bubble cloud behavior in a cavitating jet impinged vertically on a wall, which was captured with a high-speed video camera (9). The measured collapse time of the bubble cloud near the wall surface was about 50 to 150 microseconds, which was analyzed from successive image frames. The predicted time for the bubbles to shrink was shorter than the measured collapse time since we simulated isolated bubble behavior without collapsing, and the jet velocity and

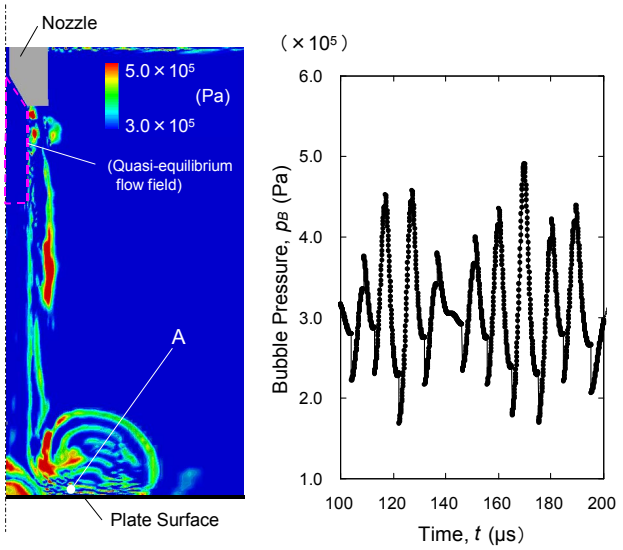

(a) Bubble pressure (b) Time variation in bubble pressure at point A

Fig. 4 Bubble pressure in Case 1

the surrounding water pressure were higher than those in the experiment conducted by Sato et al.. However, the time scale for the bubble pressure fluctuations in the simulation was valid.

Figure 5 shows the energy density of the cavitation collapse energy obtained from Eq. (10), i.e., $E/\Delta V$. The cavitation energy was high in the region (indicated by arrow B) around the jet center axis and in the other peripheral region (indicated by arrow C) away from the jet center axis near the plate surface. When the cavitating jet is impinged vertically

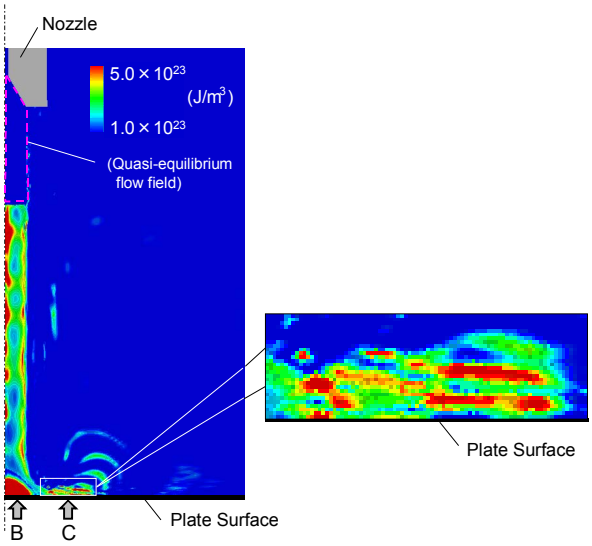

Fig. 5 Cavitation collapse energy in Case 1

on the flat plate, the occurrence of ring-like erosion has been observed on the material surface (e.g., by Sato et al. (9)). The peripheral region indicated by arrow C has a correlation with the ring-like erosion.

Cavitation Collapse Energy and Compressive Residual Stress

The correlation between the estimated cavitation collapse energy and the measured compressive residual stress on the flat plate after WJP was investigated in Cases 2-5. We used a stainless steel plate, on which tensile residual stress was introduced by grinding before WJP. The X-ray residual stress measurement was conducted on the flat plate after WJP.

The inlet velocity and the standoff distance were different in Cases 2-5 while the pressure boundary condition was fixed at 1.0×10^5 Pa since the water depth at the plate was below 1 m in the experiment. The cavitation collapse energy that acted vertically on the plate surface and caused the plastic deformation was estimated in the present study,

$$E_{surf} = \alpha \frac{E}{\Delta S}\left(\frac{T_{\exp}}{\Delta T}\right) = \sum_{p_{Bi}>p_{Bith}} \alpha\, p_{Bi}^{\,2}(n_G \Delta z)\left(\frac{T_{\exp}}{\Delta T}\right) \quad , \quad (11)$$

where T_{exp} is the jet injection time. T_{exp} was 2 minutes without moving the nozzle in the experiment. The ΔS is the cross-section of each numerical mesh on the plate surface. Equation (11) means the energy per unit cross-section, which was summed up in the direction of the jet center axis, i.e., in the z direction since the cartesian mesh in the r-z plane was used. The α is a damping coefficient depending on the vertical distance from the plate surface (18),

$$\alpha = e^{-\left(\frac{4}{3}\right)\left(\frac{\omega^2}{\rho c^3}\right)\mu d} \quad , \quad (12)$$

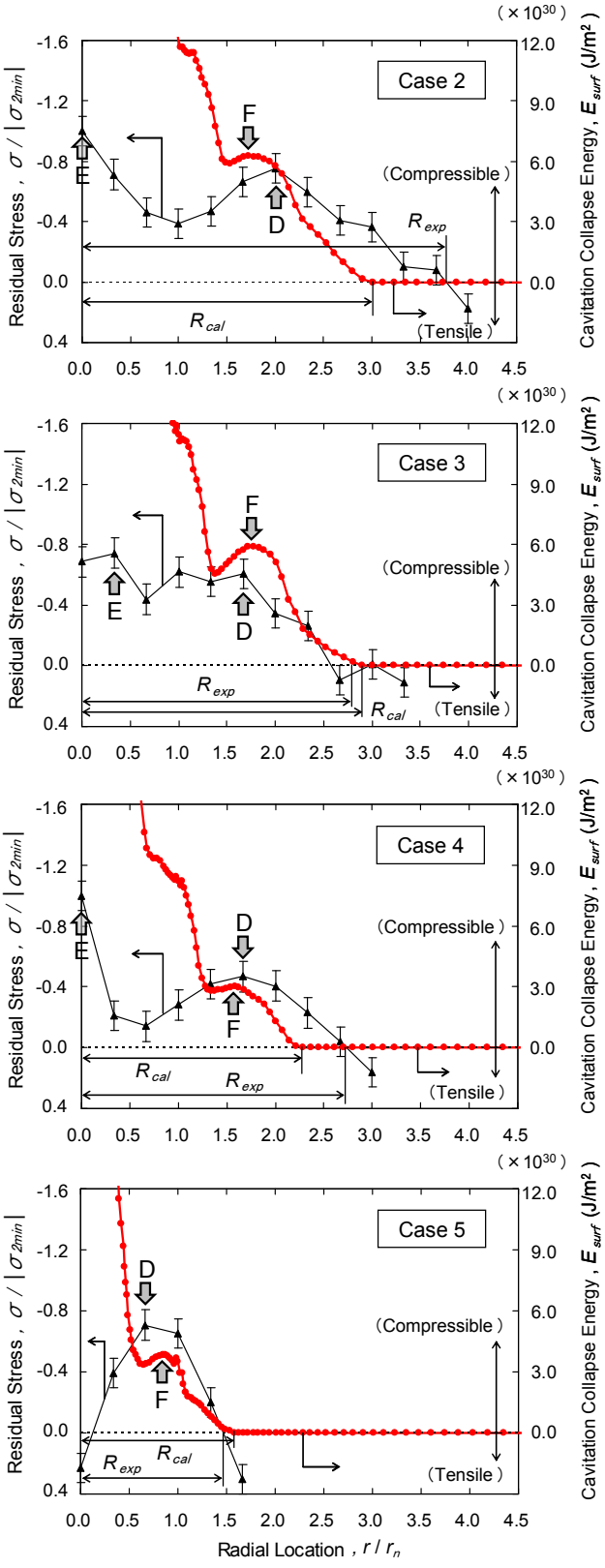

Fig. 6 Comparison between predicted cavitation collapse energy and measured residual stress in Cases 2-5

where ω is the pressure wave frequency, c is the sonic velocity in water including bubbles, and d is the vertical distance between the bubble collapse location and the plate surface. $\omega = 1.0 \times 10^7$ Hz and c= 30 m/s were temporarily derived; then, the cavitation collapse energy was damped to be about 10 % when d was 50 mm. The adding up in Eq. (11) was conducted when the bubble pressure exceeded the threshold value since only high cavitation collapse energy caused plastic deformation of the material surface (17, 13, and 14). The bubble pressure threshold was temporarily assumed to be 1.02×10^5 Pa in the simulation.

Figure 6 compares the cavitation collapse energy calculated from Eq. (11) and the measured residual stress in Cases 2-5. The radial location, r, and the residual stress, σ, were simultaneously nondimensionalized by the nozzle radius, r_n, and the absolute value of the minimum residual stress in Case 2. Compressible residual stress was introduced to the stainless steel plate by WJP, and this was distributed within a radial range from the jet center axis. The distribution of compressible residual stress had a peak, indicated by arrow D, away from the jet center axis. The peak indicates the strong impacts caused by cavitation bubble collapses and the correlation with ring-like erosion (e.g., by Sato et al. (9)). The other peak indicated by arrow E was caused not only by bubble collapse impacts but also by the high-speed impingement of water. No peak appeared in Case 5 since the jet velocity was too low.

The distribution of cavitation collapse energy also had a peak indicated by arrow F similar to that indicated by arrow D. Figure 7 compares the radial locations and the values of peaks indicated by arrows D and F in Fig. 6. The radial peak location of compressive residual stress in Case 5 was remarkably near the jet center axis compared with the other Cases 2-4. The peak value of compressive residual stress was lowest in Case 4. The cavitation collapse energy also had similar tendencies.

The simulation could not predict the values of peaks indicated by arrows E in Fig. 6. The cavitation collapse energy was exceedingly overestimated when the radial location was below about 1.4 in Cases 3-5 or below 0.6 in Case 6. There were two main causes.

(i) The static pressure of water around the flow stagnation point on the flat plate and the jet center axis was much too high since turbulent flow diffusion was not taken into account in the simulation, and the actual strong unsteadiness of flow was also not simulated. The overestimated water pressure surrounding the bubble enormously increased the bubble pressure through Eq. (4).

(ii) The damping effect modeled with Eq. (12) was underestimated.

The radial range of compressive residual stress from the jet center axis, R_{exp}, is one of the most important measures of performance of WJP, and R_{exp} ranged from 1.5 to 3.7, as shown in Fig. 6. Figure 8 compares R_{exp} and R_{cal}. The R_{cal} is the radial range of the cavitation collapse energy in Fig. 6, and ranged from 1.6 to 3.0. The R_{exp} and R_{cal} decreased when the standoff distance was shorter in Cases 2 and 3. The R_{exp} and R_{cal} also

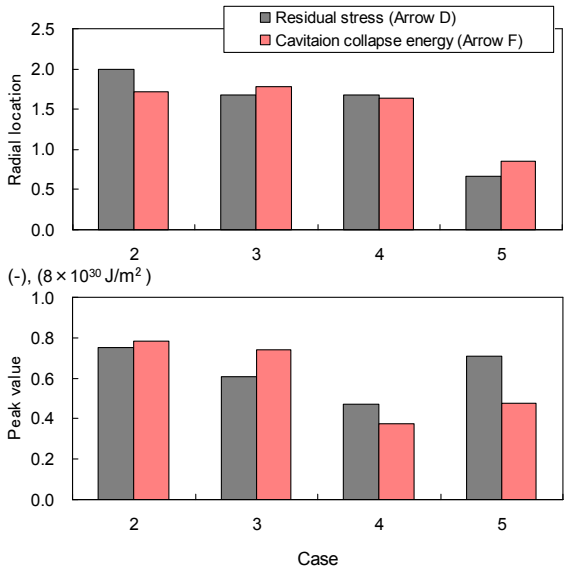

Fig. 7 Radial location and value of distribution peak of compressive residual stress and cavitation collapse energy in Fig. 6

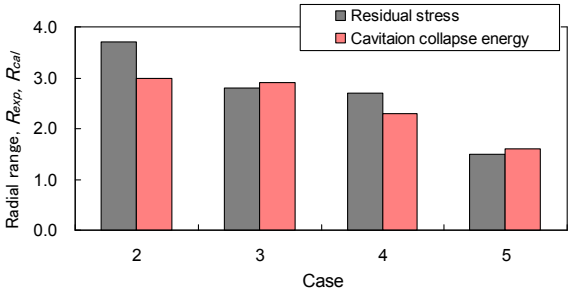

Fig. 8 Radial range of compressive residual stress and cavitation collapse energy in Fig. 6

decreased when the inlet velocity was decreased in Cases 3-5. The R_{cal} corresponded to R_{exp} with a prediction error of +/s 20% in Cases 2-5. The results demonstrated that the numerical method we developed for predicting the region of compressive residual stress after WJP was valid.

CONCLUSION

The cavitation collapse energy was numerically predicted by using the bubble flow model to estimate the compressive residual stress introduced by WJP. The cavitating jet impinging vertically on the submerged flat plate was simulated. The distributions of the predicted cavitation collapse energy and the measured compressive residual stress on the stainless steel plate surface were compared. We found:

(1) Both distributions had a ring-like peak around the jet center axis, which was similar to the ring-like cavitation erosion observed in the previous studies.

(2) A comparison of the distributions was conducted while changing inlet velocity and the distance between the nozzle and the flat plate. The radial range of the cavitation collapse energy from the jet center axis corresponded to that of compressive residual stress with a prediction error of +/- 20%.

The results proved that the numerical method we developed worked in practice to predict the performance of WJP, i.e., the radius of the circular region where residual stress was improved by WJP.

REFERENCES

(1) Mochizuki, M., et al., 1993, "A Study on Residual Stress Improvement by Water Jet Peening," Proc. of the 5th Int. Conf. on Shot Peening, Oxford, United Kingdom, pp. 247-256.

(2) Anzai, H., et al., 1999, "Residual Stress Improvement of BWR Core Shroud for IGSCC Mitigation Using Water Jet Peening Technology," PLIM+PLEX Conference, Madrid, Spain.

(3) Hirano, K., et al., 1997, "Improvement of residual stress on material surface by water jet peening," Trans. of the 14th Int. Conf. on Structural Mechanics in Reactor Technology (SmiRT 14), Lyon, France, D02/4.

(4) Sagawa, W., et al., 2000, "Application of Water Jet Peening Technology to BWR Core Shroud for IGSCC Mitigation," Proc. of the 8th Int. Conf. on Nuclear Engineering, Baltimore, ICONE-8311.

(5) Hirano, K., et al., 2000, "Residual Stress Improvement by Oblique Water Jet Peening," Proc. of the 9th Int. Conf. on Pressure Vessel Technology, Sydney, Vol. 2, pp. 599-605.

(6) Knapp, R. T., et al., 1970, "Cavitation," Engineering Societies Monographs, McGraw-Hill, pp. 321-356.

(7) Soyama, H., et al., 2000, "Use of Cavitating Jet for Introducing Compressive Residual Stress," Trans. of the ASME, J. of Manufacturing Science and Engineering, Vol. 122, Issue 1, pp. 83-89.

(8) Soyama, H., et al., 2004, "Compressive Residual Stress into Titanium Alloy Using Cavitation Shotless Peening Method," Tribology Letters, Vol. 17, No. 3, pp. 501-504.

(9) Sato, K., et al., 2009, "Pressure-Wave Formation and Collapses of Cavitation Clouds Impinging on Solid Wall in a Submerged Water Jet," Proc. of the 7th Int. Symposium on Cavitation, CAV2009, Ann Arbor, Paper No. 66.

(10) Soyama, H., et al., 2009, "Enhancement of Cavitation Aggressivity around a Cavitating Jet by Injecting Low-Speed Water Jet for Cavitation Peening," Proc. of the 7th Int. Symposium on Cavitation, CAV2009, Ann Arbor, Paper No. 12.

(11) Shinbo, K., 2007, "Propagating Behavior of Elastic Waves in Solid Caused by Bubble Collapse," Proc. of the 7th Int. Symposium on Advanced Fluid Information and 4th Int. Symposium on Trasdisciplinary Fluid Integration, pp. 256-259.

(12) Plesset, M. S., 1954, "On the Stability of Fluid Flows with Spherical Symmetry," J. Appl. Phys., 25, pp. 96-98.

(13) Fukaya, M., et al., 2010, "Prediction of Cavitation Intensity and Erosion Area in Centrifugal Pump by Using Cavitating Flow Simulation with Bubble Flow Model," J. of Fluid Science and Technology, Vol. 5, No. 2. (to be published)

(14) Fukaya, M., et al., 2009, "Prediction of Impeller Speed Dependence of Cavitation Intensity in Centrifugal Pump Using Cavitating Flow Simulation with Bubble Flow Model," Proc. of the 7th Int. Symposium on Cavitation, CAV2009, Ann Arbor, Paper No. 15.

(15) Tamura, Y., et al., 2002, "Numerical Method for Cavitating Flow Simulations and its Application to Axial Flow Pumps," Proc. of the 9th Int. Symposium on Transport Phenomena and Dynamics of Rotating Machinery (ISROMAC-9), Honolulu, FD-ABS-129.

(16) Takemura, F. and Matsumoto, Y., 1994, "Internal Phenomena in Bubble Motion," Bubble Dynamics and Interface Phenomena, KLUWER, pp. 467-474.

(17) Soyama, H. and Kumano, H., 2002, "The fundamental threshold level – a new parameter for predicting cavitation erosion resistance," Journal of Testing and Evaluation, ASTM International, pp. 421-431.

(18) Dular, M., et al., 2006, "Development of a cavitation erosion model," Wear, Vol. 261, No. 5-6, pp. 642-655.